LETTERS
PUBLISHED ONLINE: 27 FEBRUARY 2011 | DOI: 10.1038/NPHOT.2011.18
nature photonics

Optofluidic modulator based on peristaltic nematogen microflows

J. G. Cuennet[1†], A. E. Vasdekis[1*†], L. De Sio[2] and D. Psaltis[1]

Nematogens rotate by the application of external fields, thereby enabling optical modulation. This principle has had a profound impact on our daily lives through the plethora of liquid-crystal displays in use around us[1,2]. However, the wider use of nematic liquid crystals, particularly in microdisplays[3] and information processing, has been hampered by their slow response times. In nematogens, rotational and translational molecular motions are coupled[4], so flow is inevitably linked with optical modulation[5,6]. This linkage motivated us to fuse microfluidics with anisotropic liquids and introduce an optofluidic[7,8] modulator that exhibits a submillisecond (250 μs) symmetric response and can operate at frequencies up to 1 kHz. The modulator is based on peristaltic nematogen microflows[9] realized in polydimethylsiloxane microfluidics. The latter simultaneously permits peristalsis by means of elastomeric deformation, nematogen alignment and rapid prototyping through cast-moulding. Together with large-scale, vertical integration and piezoelectric nanotechnologies, this optofluidic paradigm can enable high-density and three-dimensional architectures of fast modulators.

The term 'optofluidics'[7,8] emerged in 2003 to describe the fusion of microfluidics and integrated optics, which found application in novel photonic devices such as microscopes, particle manipulators and light sources[10–12]. Reconfiguration in optofluidics primarily stems from mixing fluids, or interfacing them with other liquids and surfaces. However, optofluidics based on anisotropic liquids has received little attention[13]. Nematic liquid crystals (NLCs), a widely used anisotropic fluid, have been explored for more than a century because of their fascinating soft-condensed matter nature and unique optical properties[14,15]. As a result, a plethora of practical optical devices have been developed, including displays (LCDs)[1,2], memories[16] and resonators[17]. However, significant improvement is essential in the areas of speed and integration in three dimensions if NLCs are to maintain their comparative advantage over emerging technologies. NLC performance is limited due to their mechanical character, which usually results in long and asymmetric response times. Despite the advent of ferroelectric liquid crystals[18] and novel composite liquid-crystal media[19–21], pure nematogens remain attractive because of their simplicity, low cost and significant expertise in alignment methods. Rapid prototyping of three-dimensional architectures would further enhance the development of related applications of NLC-based devices[22].

To address the slow NLC response and limited device architectures, we pursued an optofluidic strategy through the direct flow of NLCs in polydimethylsiloxane (PDMS) microfluidic channels. An integrated high-frequency mechanical oscillator embedded in the channel inlet enabled peristaltic flow by means of local channel volume modulation[9,23,24], capable of operating at frequencies up to 1 kHz. Flow, in turn, caused periodic NLC director profile orientation and therefore optical modulation. NLC translational motion is coupled to inner rotational molecular motions[4,15] through the introduction of viscous torques by the velocity gradient (along the z-axis in Fig. 1a); this effect has been used in the past to probe fundamental NLC properties[5,6,25]. The expected director profile is plotted in Fig. 1a. Such alignment may not induce the highest possible birefringence (compared, for example, to a uniform director angle profile); however, it is inevitably linked with nematogen Poiseuille flow in the microchannels[5,6,23]. The microfluidic chips were realized in PDMS by cast-moulding (see Methods). Figure 1b shows images of the E7-filled channels. Under no flow, the channel appears dark due to the perpendicular (homeotropic) alignment of the NLC, as was also confirmed by conoscopy. The E7 constituents contain non-polar alkyl tails and polar cyano heads and are therefore aligned perpendicularly due to the hydrophobicity of the PDMS boundary conditions[26]; this alignment is perturbed under flow, causing the channel to appear bright.

To identify the optimal microfluidic geometry, we performed a steady-state experimental analysis by introducing the E7 into channels with varying cross-sectional dimensions. For channels with widths greater than their heights, E7 aligned homeotropically. When the channel height was comparable to its width, the orthogonal channel surfaces (x–y and x–z planes; Fig. 2a, inset) imposed a perpendicular torque, perturbing the alignment (Fig. 2a, inset). The homeotropic area variation as a function of channel width exhibits a clear threshold, which is smaller for thinner channels (Fig. 2a). Below threshold, the alignment is planar due to the stronger alignment condition in the y–z plane. Above threshold, the homeotropic area increases until saturation, a behaviour analogous to the Freedericksz transition[27]. Closer to the channel edges, a defect occurs, manifesting itself as a bright area, indicating a localized director reorientation (Fig. 2a, inset). To avoid interference between the surface and hydrodynamic forces, we operated well above threshold, within the saturation regime, where flow can be considered Poiseuille-type[6,23]. To achieve maximum flow rates, we used the largest possible channel dimensions (8 μm × 130 μm, unless stated otherwise), limited only by the channel structural stability[28].

To enable peristalsis, a metallic needle was fixed at one end at the loudspeaker, and the other end was inserted into the channel inlet. When a square pulse actuates the loudspeaker, friction forces appear between the needle and the inlet sidewalls, resulting in microchannel deformation (Fig. 1a, lower panel). When the needle moves downwards ('push' state), the microchannel volume decreases, pushing the NLCs towards the inlet[23]. The volume increases when the needle moves upwards ('pull' state), introducing more NLCs into the channel. As a result, alternating backward and forward NLC flows occur[23]. Silver particles dispersed in the PDMS used to form the microchannels allowed us to directly measure elastomer deformations of up to 0.5 μm in the plane parallel to the flow[29].

[1]Optics Laboratory, School of Engineering, Swiss Federal Institute of Technology Lausanne (EPFL), CH-1015 Lausanne, Switzerland, [2]LICRYL (Liquid Crystals Laboratory, IPCF-CNR), Center of Excellence CEMIF.CAL and Department of Physics, University of Calabria, 87036 Arcavacata di Rende (CS), Italy;
[†]These authors contributed equally to this work. *e-mail: andreas.vasdekis@epfl.ch

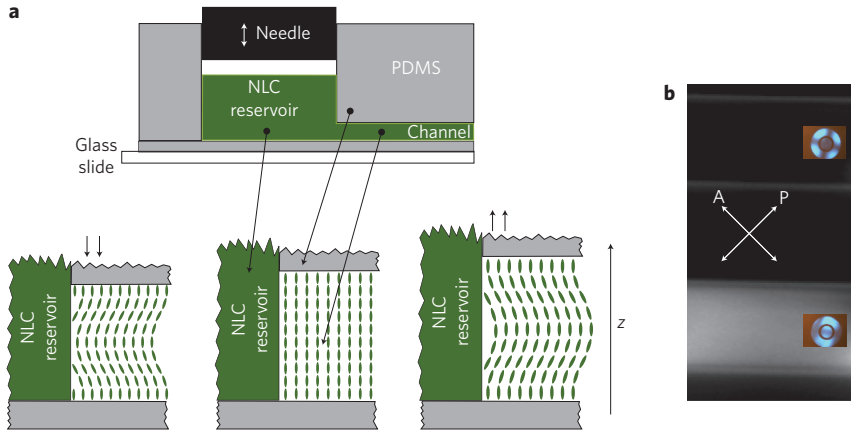

Figure 1 | Concept of peristaltic flows of nematogens in microfluidic channels. a, Upper panel: schematic of the microfluidics coupled to the speaker; lower panel: effect of peristalsis. **b**, Two transmission states of 100-μm-wide channels between crossed polarizers in the absence (upper) or presence (lower) of flow. Insets: respective conoscopic measurements.

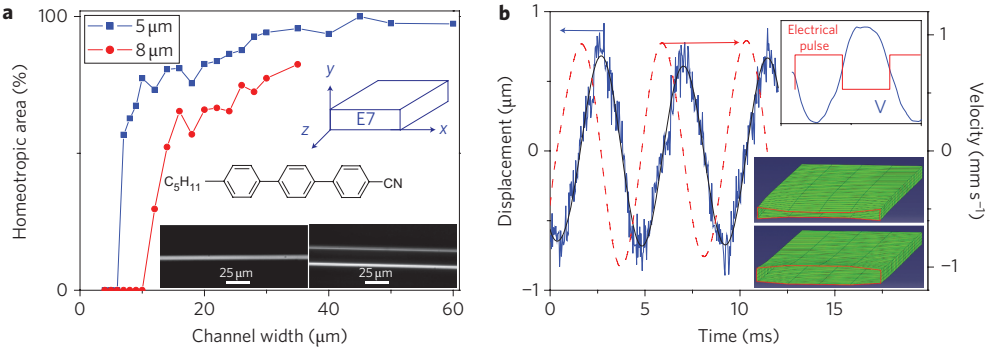

Figure 2 | Steady-state analysis of nematogens in confined geometries and peristaltic flow visualization. a, Homeotropic area dependence on channel width. Insets: microfluidic channel geometry, molecular structure of one of the E7 constituents and two transmission images of two 8-μm-thick channels with widths of 7 μm (left) and 25 μm (right). **b**, Particle trajectories under peristalsis. Upper inset: volume change within one cycle (amplitude, 600 μm^3) and the electrical pulse driving the loudspeaker at a frequency of 250 Hz. Lower inset: volume change in the channels under peristalsis (amplified by a factor of 10).

A viscous liquid doped with the same particles was introduced inside the microfluidics to reveal the flow inside the channels; typical results are shown in Fig. 2b for a frequency of 250 Hz, demonstrating particle velocities up to 1 mm s^{-1}. The three-dimensional channel deformations were computed using time-domain numerical analysis (Abaqus/Explicit; see Methods), where the recorded PDMS strain field was introduced as the input perturbation. Typical deformation snapshots are shown in the inset to Fig. 2b at a frequency of 250 Hz. The numerical analysis revealed that flow rates and velocities up to 0.01 μl s^{-1} and 9.5 mm s^{-1}, respectively, are feasible. The discrepancy between the experimental and calculated flow velocity is primarily attributed to the viscous losses associated with peristaltic flow, which are not accounted for in our numerical model, and also to the limited precision in measuring the load under peristalsis.

The oscillatory peristaltic flow translates into a periodically modulated optical retardation and transmission through the microfluidic cell. This was measured by placing the microfluidic cells between crossed polarizers (Fig. 3a). A typical transmission measurement is shown in Fig. 3b (blue), together with the electrical pulse train (black) used to actuate the loudspeaker at 178 Hz. Within one peristaltic cycle, two transmission peaks can be identified; under no flow conditions (steady state), the transmission is zero (red) with a maximum contrast of 16. The two peaks within one peristaltic cycle are attributed to the positive and negative volume change and thus the forward and backward flow, respectively. The rise and fall times were submillisecond and approximately symmetric (Fig. 3b, inset). The rapid and symmetric responses are attributed to the fast peristaltic flow switching enabled by direct actuation of the channel walls. To our knowledge, no other nematogen actuation method has reported both submillisecond and symmetric response times[30]. In addition, other than recent reports on integrated resonator approaches, fast optofluidic switching has received little attention[31]. To confirm the underlying modulation mechanism, we performed transmission experiments by directly connecting the loudspeaker to the membrane of a custom-made syringe pump. The time response was found to be similar to the peristaltic response (Fig. 3c). We note, however, that with the direct syringe method, it was not possible to achieve high-frequency operation due to the losses and dispersion associated with the viscoelasticity of the intermediate connecting parts[29]; these losses are not significant in the substantially more integrated peristaltic technique. The anticipated velocity and director profiles under peristaltic flow are plotted in the inset of Fig. 3c; these were calculated by linking the flow with the bend torques due to the nematogen orientation itself[5,6].

The optofluidic modulator was capable of operating at 1 kHz. Figure 4a shows two transmission frames corresponding to dark and bright states with a time difference of 500 μs (see also Supplementary Information). For this measurement, the rise and fall times were 250 and 290 μs, respectively (Fig. 4a). The optical transmission was localized within ~200 μm from the inlet. Closer to the inlet (55 μm), the forward flow transmission peak is split into two (Fig. 4c). The two peaks converge back into one at larger distances from the inlet (130 μm), with a much lower amplitude further

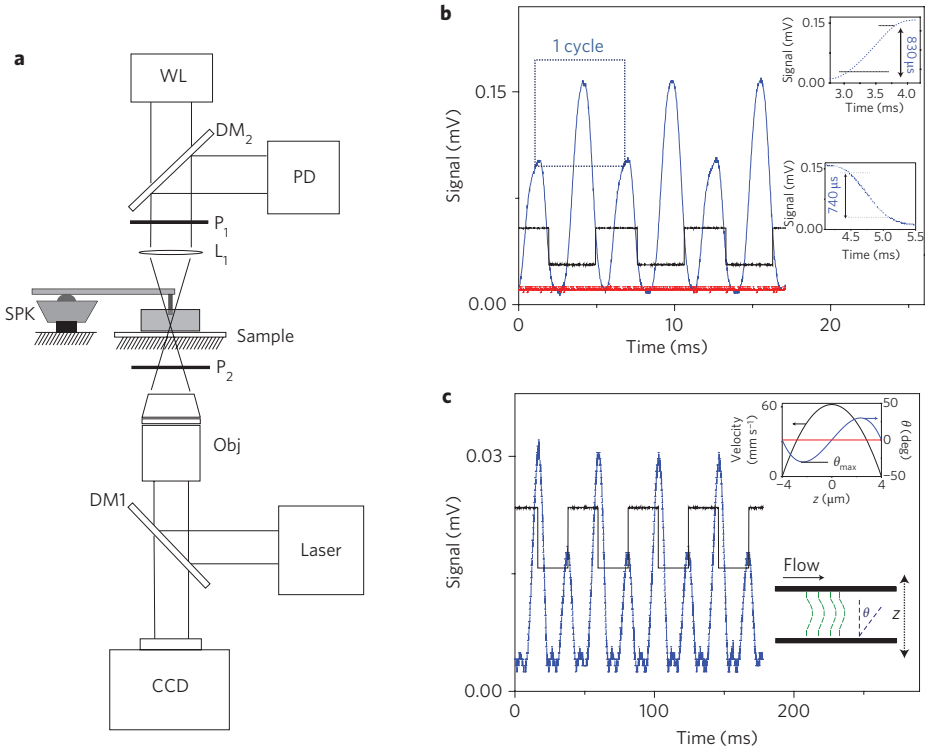

Figure 3 | Optical modulation. a, Optical set-up. WL, white light source; PD, photodiode; SPK, speaker; $P_{1,2}$, polarizers; L_1, lens; Obj, objective; DM, dichroic mirror. **b**, Transmission at 178 Hz under steady state (red) and peristalsis (blue), together with the driving pulse (black). Inset: magnified on and off profiles. **c**, Transmission data as in **b**, with flow induced by a syringe pump. Inset: calculated Poisseuille velocity profile (black) and corresponding director profiles for two velocity profiles under zero flow (red) and peristalsis (blue).

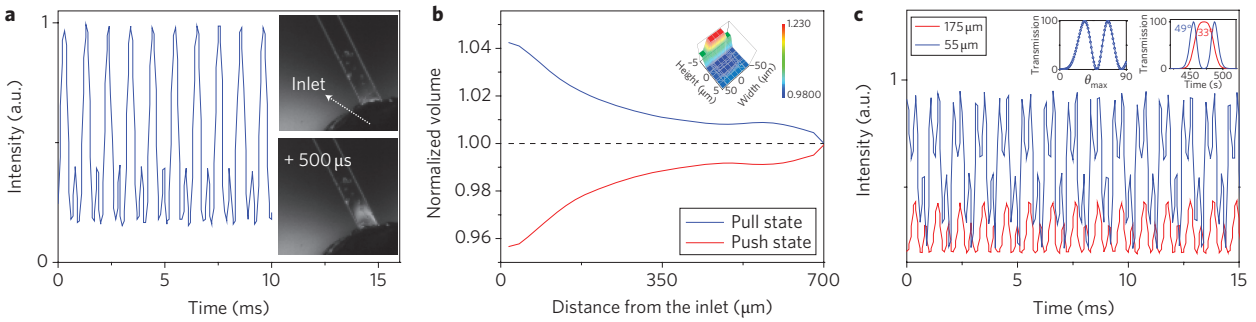

Figure 4 | Performance at 1 kHz. a, Transmission at 130 µm from the inlet (70 µm × 8 µm channel). Inset: two transmission frames at 0 µs and 500 µs. **b**, Volume variation at increasing distances from the inlet under the experimentally determined load of 15 kN m^{-2}. Inset: simulated normalized volume deformation at the inlet. **c**, Transmission experiments at two different distances from the vibrating inlet. Insets: calculated transmission at 488 nm as a function of the maximum director angle (θ_{max}) in the microchannel and as a function of time for two different θ_{max}.

away (175 µm). The appearance of a double maximum of the optical signal manifests that phase retardation higher than π occurs (Fig. 4c, inset). Similar behaviour is observed at lower frequencies (320 Hz) for the same modulator (Supplementary Section 2). Numerical analysis at this frequency revealed that the peristaltic channel volume deformation is inversely proportional to the distance from the perturbation source (Fig. 4b), thereby explaining the distance-dependent phase retardation. By reducing the channel volume deformation by ~30%, the double transmission peaks converge back to a single one, even close to the inlet (Supplementary Section 3). The distance-dependent channel volume deformation represents a simple method to confine the active modulation area in two dimensions, hence creating an individual pixel.

NLC cells placed between crossed polarizers induce maximum intensity modulation at an optical path difference of an odd multiple of π (ref. 15). In our system, this condition is estimated to occur when the maximum director angle (θ_{max} in Fig. 3c) is ~33°, as plotted in the inset of Fig. 4c (refs 5 and 6). We have observed this for frequencies up to 1 kHz (Fig. 4c), suggesting that peristaltic microflows can tilt the NLC director at high enough angles that the maximum possible useful phase modulation can be achieved. However, we measure extinction ratios of only up to around 33; this is limited by the inherent birefringence of the deformed PDMS due to the integrated needle[32]. Between crossed polarizers, PDMS deformation is manifested as the bright areas observed in the insets of Fig. 4a in the proximity of the inlet, both under equilibrium or peristaltic conditions. The inherent PDMS strain is expected to decrease the extinction ratio of our modulator by partially depolarizing the incident radiation. This was addressed by placing the actuation needle further away from the channel inlet

(~3 mm), therefore minimizing PDMS strain in the region of the microflows. In this case, peristalsis induced optical contrasts of up to 200 (Supplementary Section 4).

In conclusion, we have demonstrated that peristaltic flow can force rapid nematogen orientation and have introduced a flow-driven optical modulator with a response that is both submillisecond and symmetric up to 1 kHz. In contrast to conventional pressure-driven methods, peristalsis allows for rapid oscillatory flows and realization of micrometre-scale optical modulators. Together with the emerging piezoelectric nanotechnologies[33], we propose this optofluidic paradigm for fast, cost-effective and compact modulators. Piezoelectric peristaltic micropumps and composite elastomeric media can enable an enhancement in speed through faster actuation and tailored strain field application, respectively. Other advantages of our method are that multilayer soft lithography can allow vertical, large-scale integration of such NLC devices with microfluidic circuits for three-dimensional displays, as well as novel analytical and imaging methods[34].

Methods

Materials and fabrication. PDMS microfluidic chips were fabricated using conventional soft lithography. Negative photoresist SU-8 (GM-1040, Gersteltec) on a silicon wafer was patterned by means of optical lithography. The structured SU-8 was treated with trimethylchlorosilane vapour for 2 min (TMS, Sigma Aldrich) and the pattern was transferred to the PDMS (Dow Corning Sylgard 184, Omya AG, monomer–catalyst ratio of 10:1) by cast moulding. The structured and flat PDMS was placed in an O_2 plasma chamber (15 W, 20 s) to bond permanently. To avoid surface energy modification due to exposure to O_2 plasma during the bonding step, the chips were left under ambient conditions for ~24 h. After bonding, the chips were immobilized on a glass coverslip. Similar steps could be used to integrate PVA polarizers (Polaroids) on the top surface of our PDMS structure[35]. For measuring the PDMS strain, silver nanoparticles (2–3.5 μm, Sigma Aldrich) were mixed with the PDMS monomer catalyst solution at an approximate ratio of 1:700 by weight. For visualizing the microfluidic flow, the channels were filled with a viscous solution of glycerine (97%) and water (3%), mixed with the nanoparticle solution at a very low concentration to ensure single-particle imaging.

The E7 NLC (Merck) was introduced into the channels in its anisotropic state (room temperature) at the inlet through Tygon tubing (Fisher Scientific AG) and a metal tip with an inner diameter of ~0.6 mm (23G), and left to stabilize for ~10 min before flow. For channel thicknesses greater than 8 μm, the PDMS surfaces needed to be treated with an ethanol solution of polypropylene sulphide to obtain repeatable and uniform alignment. Note that it was not possible to align cholesteric (CLC BL088, Merck; helix pitch, 400 nm) and ferroelectric (CS-1024 FLC, Chisso) liquid crystals on PDMS, or SiO-coated PDMS, with no additional chemical treatments. The inlet was connected through a similar needle to a loudspeaker (Monacor, SPH-8XTB), placed ~0.5 m away to avoid any direct vibrations. The optical transmission peaks due to the backward and forward flow were asymmetric in amplitude in both the peristaltic and direct flow measurements, suggesting the presence of an asymmetric forward and backward motion in the speaker. In addition, the rise and fall profiles of the NLC were found to be dependent on the loudspeaker frequency. This is due to the frequency dependence of the amplitude response of the loudspeaker itself.

Experimental set-up. The chips were investigated on an inverted frame microscope (Olympus IX71) equipped with a high-resolution stage (MS-2000, Applied Scientific Instrumentation) and phase contrast objectives (Olympus, UPLFLN 4 × PH and 10 × PH). The chips were placed between crossed polarizers, oriented at ±45° with respect to the flow direction. Images and videos were captured with an electron multiplying charge coupled device (EMCCD) camera (iXon DV885 VP, Andor Technology) or a fast charge-coupled device (CCD) camera (Phantom v710 mono, Vision Research). The laser experiments were performed using the 488 nm line of an argon ion laser (Innova 300, Coherent), collected by a biased silicon photodiode (ET2000, Electro-Optics Technology) with fast rise (<200 ps) and fall (<350 ps) times. Contrast was evaluated according to the 10–90% criterion.

Theoretical strategy. Calculations regarding liquid crystal orientation and optical transmission were performed on a model described in refs 6 and 36. The time-domain calculations of Fig. 4c are approximate, based on the assumption that the perturbation is very long, allowing for the steady state to be reached within its duration. The time-domain numerical analysis of channel volume deformation was carried out using the commercial software Abaqus/Explicit. For this, the model included the microfluidic channel (10 μm × 100 μm) embedded inside a three-dimensional PDMS block (8 mm × 8 mm × 4 mm), where the upper and lower boundary conditions were that of free and bound surfaces, respectively. The meshing was performed with explicit linear elements (C3D8R, an eight-node linear brick, reduced integration and hourglass control) with a finer seeding around the microchannel. At one end of the channel, a hole was created (0.6 mm in diameter) and a metallic needle was placed to perform the actuation. The channel was filled with a solid with a very low Young's modulus (3×10^{-5} Pa) and a high Poisson coefficient (0.5) to mimic the viscous liquid used in experimentation. The needle actuation load was experimentally determined by directly measuring the PDMS strain at a single location and numerically varying the load until the calculated deformation matched the experimental one.

Received 8 November 2010; accepted 21 January 2011; published online 27 February 2011

References

1. Gibbons, W. M., Shannon, P. J., Sun, S. T. & Swetlin, B. J. Surface mediated alignment of nematic liquid-crystals with polarized laser-light. *Nature* **351,** 49–50 (1991).
2. Schadt, M., Seiberle, H. & Schuster, A. Optical patterning of multidomain liquid-crystal displays with wide viewing angles. *Nature* **381,** 212–215 (1996).
3. Vettese, D. Liquid crystal on silicon. *Nature Photon.* **4,** 752–754 (2010).
4. De Gennes, P. G. & Prost, J. *The Physics of Liquid Crystals* 198 (Oxford Science Publications, 1993).
5. Jewell, S. A., Cornford, S. L., Yang, F., Cann, P. S. & Sambles, J. R. Flow-driven transition and associated velocity profiles in a nematic liquid-crystal cell. *Phys. Rev. E* **80,** 041706 (2009).
6. Waton, G., Ferre, A., Candau, S., Perbet, J. N. & Hareng, M. Characterization of distortions induced by a flow or an electric field in nematics using conoscopic measurements *Mol. Cryst. Liq. Cryst.* **78,** 237–249 (1981).
7. Psaltis, D., Quake, S. R. & Yang, C. H. Developing optofluidic technology through the fusion of microfluidics and optics. *Nature* **442,** 381–386 (2006).
8. Monat, C., Domachuk, P. & Eggleton, B. J. Integrated optofluidics: a new river of light. *Nature Photon.* **1,** 106–114 (2007).
9. Unger, M. A., Chou, H. P., Thorsen, T., Scherer, A. & Quake, S. R. Monolithic microfabricated valves and pumps by multilayer soft lithography. *Science* **288,** 113–116 (2000).
10. Cui, X. Q. *et al.* Lensless high-resolution on-chip optofluidic microscopes for *Caenorhabditis elegans* and cell imaging. *Proc. Natl Acad. Sci. USA* **105,** 10670–10675 (2008).
11. Yang, A. H. J. *et al.* Optical manipulation of nanoparticles and biomolecules in sub-wavelength slot waveguides. *Nature* **457,** 71–75 (2009).
12. Song, W. Z., Vasdekis, A. E., Li, Z. Y. & Psaltis, D. Optofluidic evanescent dye laser based on a distributed feedback circular grating. *Appl. Phys. Lett.* **94,** 161110 (2009).
13. Haakestad, M. W. *et al.* Electrically tunable photonic bandgap guidance in a liquid-crystal-filled photonic crystal fiber. *IEEE Photon. Tech. Lett.* **17,** 819–821 (2005).
14. Reinitzer, F. Beitrage zur Kenntniss des Cholesterins. *Monatsh. Chemie* **9,** 421–425 (1888).
15. Khoo, I. C. *Liquid Crystals: Physical Properties and Nonlinear Optical Phenomena* (Wiley, 1995).
16. Ikeda, T. & Tsutsumi, O. Optical switching and image storage by means of azobenzene liquid crystal films *Science* **268,** 1873–1875 (1995).
17. Humar, M., Ravnik, M., Pajk, S. & Musevic, I. Electrically tunable liquid crystal optical microresonators. *Nature Photon.* **3,** 595–600 (2009).
18. Kurokawa, T. & Fukushima, S. Spatial light modulators using ferroelectric liquid-crystal. *Opt. Quant. Electron.* **24,** 1151–1163 (1992).
19. Khoo, I. C., Park, J. H. & Liou, J. D. Theory and experimental studies of all-optical transmission switching in a twist-alignment dye-doped nematic liquid crystal. *J. Opt. Soc. Am. B* **25,** 1931–1937 (2008).
20. Castles, F., Morris, S. M., Gardiner, D. J., Malik, Q. M. & Coles, H. J. Ultra-fast-switching flexoelectric liquid-crystal display with high contrast. *J. Soc. Inf. Display* **18,** 128–133 (2010).
21. Jewell, S. A. & Sambles, J. R. Dynamic response of a dual-frequency chiral hybrid aligned nematic liquid-crystal cell. *Phys. Rev. E* **73,** 011706 (2006).
22. Blanche, P.-A. *et al.* Holographic three-dimensional telepresence using large-area photorefractive polymer. *Nature* **468,** 80–83 (2010).
23. Jaffrin, M. Y. & Shappiro, A. H. Peristaltic pumping. *Annu. Rev. Fluid Mech.* **3,** 13–37 (1971).
24. Smits, J. G. Piezoelectric micropump with 3 valves working peristatically. *Sensor Actuat. A* **21,** 203–206 (1990).
25. Pasechnik, S. *et al.* Oscillating Poiseuille flow in photo-aligned liquid crystal cells. *Liq. Cryst.* **33,** 1153–1165 (2006).
26. Choi, M. C. *et al.* Ordered patterns of liquid crystal toroidal defects by microchannel confinement. *Proc. Natl Acad. Sci. USA* **101,** 17340–17344 (2004).
27. Barbero, G., Madhusudana, N. V., Palierne, J. F. & Durand, G. Optical determination of large distortion surface anchoring torques in a nematic liquid-crystal. *Phys. Lett. A* **103,** 385–388 (1984).
28. McDonald, J. C. *et al.* Fabrication of microfluidic systems in poly(dimethylsiloxane). *Electrophoresis* **21,** 27–40 (2000).
29. Wunderlich, B. K., Klessinger, U. A. & Bausch, A. R. Diffusive spreading of time-dependent pressures in elastic microfluidic devices. *Lab Chip* **10,** 1025–1029 (2010).

30. Boamfa, M. I., Lazarenko, S. V., Vermolen, E. C. M., Kirilyuk, A. & Racing, T. Magnetic field alignment of liquid crystals for fast display applications. *Adv. Mater.* **17,** 610–614 (2005).
31. Shamai, R. & Levy, U. On chip tunable micro ring resonator actuated by electrowetting. *Opt. Express* **17,** 1116–1125 (2009).
32. Hoshino, K. & Shimoyama, I. Analysis of elastic micro optical components under large deformation. *J. Micromech. Microeng.* **13,** 149–154 (2003).
33. Qin, Y., Wang, X. & Wang, Z. L. Microfibre–nanowire hybrid structure for energy scavenging. *Nature* **451,** 809–813 (2009).
34. Woltman, S. J., Jay, G. D. & Crawford, G. P. Liquid-crystal materials find a new order in biomedical applications. *Nature Mater.* **6,** 929–938 (2007).
35. Yu, L., Li, C. M., Zhou, Q. & Luong, J. H. T. Poly(vinyl alcohol) functionalized poly(dimethylsiloxane) solid surface for immunoassay. *Bioconj. Chem.* **18,** 281–287 (2007).
36. Pasechnik, S. V., Chigrinov, V. G., Shmeliova, D. V., Tsvetkov, V. A. & Voronov, A. N. Anisotropic shear viscosity in nematic liquid crystals: new optical measurement method. *Liquid Cryst.* **31,** 585–592 (2004).

Acknowledgements

The authors thank J.-F. Molinari, N. Stergiopoulos and S. Maerkl for fruitful discussions on time-domain elastomer modelling methods, oscillatory flows of viscous liquids and microfluidic flow architectures, respectively.

Author contributions

A.E.V. and D.P. conceived the peristaltic strategy. J.G.C. performed the experimental and numerical flow characterization and conoscopic measurements. A.E.V. designed the experiments, built the experimental apparatus, and performed the optical experiments, calculations and microfabrication. L.D.S. supplied background in liquid crystals and materials. A.E.V. and D.P. wrote the paper.

Additional information

The authors declare no competing financial interests. Supplementary information accompanies this paper at www.nature.com/naturephotonics. Reprints and permission information is available online at http://npg.nature.com/reprintsandpermissions/. Correspondence and requests for materials should be addressed to A.E.V.